The Astrophysical Journal, 678:1458–1470, 2008 May 10

ABUNDANCES AND ENERGY SPECTRA OF COROTATING INTERACTION REGION HEAVY IONS OBSERVED DURING SOLAR CYCLE 23

G. M. Mason,[1] R. A. Leske,[2] M. I. Desai,[3] C. M. S. Cohen,[2] J. R. Dwyer,[4] J. E. Mazur,[5]
R. A. Mewaldt,[2] R. E. Gold,[1] and S. M. Krimigis[1]
Received 2007 November 5; accepted 2008 January 17

ABSTRACT

Using instruments on the *ACE* spacecraft, we surveyed the heavy-ion spectra and composition over the range He–Fe for 41 corotating interaction regions (CIRs) during 1998–2007. Below ~1 MeV nucleon^{-1} the spectra are power laws in kinetic energy nucleon^{-1} with an average spectral index of 2.51 ± 0.10, rolling over above ~1 MeV nucleon^{-1} to power-law spectra with an average index of 4.47 ± 0.17. The spectral shapes for different species are similar, leading to relative abundances that are constant over our energy range, even though the intensities cover up to 8 orders of magnitude. Relative to oxygen, the measured abundances at 385 keV nucleon^{-1} for ^{4}He, C, N, Ne, Mg, Si, S, Ca, and Fe are 273 ± 72, 0.760 ± 0.023, 0.143 ± 0.005, 0.206 ± 0.009, 0.148 ± 0.006, 0.095 ± 0.005, 0.028 ± 0.002, 0.007 ± 0.001, and 0.088 ± 0.007, respectively. Except for an overabundance of ^{4}He and Ne, the abundances are quite close to that of the fast solar wind. We have found ^{3}He/^{4}He ratios to be enhanced over solar wind values in ~40% of the CIRs. The Fe/O ratio in individual CIRs is observed to vary over a factor of ~10 and is strongly correlated with the solar wind Fe/O ratio measured 2–4 days preceding each CIR. Taken together with previous studies showing the presence of pickup He^+ in CIRs, the observational data provide evidence that CIR energetic particles are accelerated out of a suprathermal ion pool that includes heated solar wind ions, pickup ions, and remnant suprathermals from impulsive solar energetic particle events.

Subject headings: acceleration of particles — cosmic rays — interplanetary medium — shock waves — solar wind — Sun: abundances

1. INTRODUCTION

Corotating interaction regions (CIRs) arise when fast solar wind streams overtake slower solar wind in the inner heliosphere (<few AU). The interaction between the two streams leads to enhanced levels of turbulence and the eventual formation of shocks that propagate away from the stream interface in both outward (forward) and inward (reverse) directions. Since the coronal structures giving rise to fast and slow solar wind streams may persist for months, CIRs from the same stream-stream interaction are sometimes observed for many solar rotations. Energetic particles from CIRs were observed near Earth from satellite observations in the 1960s, but it was not until a decade later that deep-space probes revealed that the peak activity in CIRs occurs at a few AU. Although much remains to be learned, a large number of observational and theoretical studies have established a basic understanding of these events (for recent reviews of plasma and energetic particle aspects of CIRs, see Fisk & Jokipii 1999; Forsyth & Marsch 1999; Gloeckler 1999; Gosling & Pizzo 1999; Horbury & Schmidt 1999; Lazarus et al. 1999; Mason & Sanderson 1999; Scholer 1999; Richardson 2004). Because particle acceleration in CIRs continues over relatively long timescales, and because the CIRs can be studied by in situ measurements, these events, in principle, should be easier to understand than other interplanetary (IP) shocks, such as those driven by coronal mass ejections (CMEs), where transient effects are important and much of the acceleration takes place remotely in the inner heliosphere.

The ion composition of the accelerated particles holds clues to understanding the details of the physical processes operating in CIRs. It has long been known that there are significant differences between the heavy-ion composition of CIRs and other heliospheric energetic particle populations, such as shock-accelerated or solar energetic particles (SEPs). Furthermore, the presence of singly ionized energetic He in CIRs makes it clear that the seed population was not simply solar wind, since solar wind He^+ is extremely rare (e.g., Gloeckler et al. 1994; Chotoo et al. 2000; Möbius et al. 2002). Using high-resolution spectrometers on the *Advanced Composition Explorer* (*ACE*) spacecraft, we have surveyed CIR events over the recent solar cycle, measuring the energy spectra and composition with much higher accuracy than previously possible. Many of the features we see have been reported previously but are established here with greater precision and a larger number of events. The primary new features revealed in this study are as follows:

1. CIRs routinely accelerate ^{3}He with an abundance several times higher than in the solar wind, showing that remnant impulsive flare suprathermal ions are accelerated in these events.
2. The average heavy-ion composition of CIR elemental abundances is very close to the average fast solar wind composition, with the exception of He and Ne, which are overabundant in CIRs by factors of approximately 3.8 and 2.9, respectively.
3. The variation of the Fe/O ratio from one CIR to the next is well correlated with the average solar wind composition observed 2–4 days earlier.

Taken together, these observations provide evidence that CIRs accelerate suprathermal ions that consist of heated solar wind bulk material and other populations, such as remnant impulsive SEP material and interstellar pickup ions. The high abundances of He and Ne might be related to their importance as pickup ions, but since previous studies have shown that most CIR-accelerated

[1] Applied Physics Laboratory, Johns Hopkins University, Laurel, MD 20723; glenn.mason@jhuapl.edu.
[2] California Institute of Technology, Pasadena, CA 91125.
[3] Southwest Research Institute, San Antonio, TX 78228.
[4] Florida Institute of Technology, Melbourne, FL 32901.
[5] The Aerospace Corporation, Chantilly, VA 20151.

He and Ne is highly ionized, a simple pickup-ion origin is not consistent with the observations.

2. OBSERVATIONS

2.1. *Instrumentation*

The observations reported here were carried out on *ACE* (Stone et al. 1998a), which was launched into an orbit around the sunward Lagrangian point in 1997. Since CIRs accelerate particles to modest energies, the bulk of the data reported here were obtained with the Ultra Low Energy Isotope Spectrometer (ULEIS; Mason et al. 1998) supplemented above ~5 MeV nucleon^{-1} by observations from the Solar Isotope Spectrometer (SIS; Stone et al. 1998b). These instruments achieve a combination of high sensitivity and mass resolution that allows determination of composition and energy spectra to a much higher level of precision than prior studies. The solar wind composition measurements reported here were obtained from the Solar Wind Ion Composition Spectrometer (SWICS; Gloeckler et al. 1998). To help identify CIR events we also used the *ACE* solar wind monitor and magnetometer (McComas et al. 1998; Smith et al. 1998).

2.2. *Event Selection*

In addition to an increase in solar wind speed, CIRs have a number of identifying features, such as an increase in solar wind plasma density and magnetic field strength (e.g., Richardson et al. 1993). While forward and reverse shocks are typical CIR features at a few AU (e.g., Desai et al. 1998), at 1 AU the shocks have often not yet formed. Most often the forward shock and its associated particles are not present, so the energetic particle spectra and abundances are dominated by particles from the reverse shock in the fast solar wind plasma portion of the event. In our survey, 18 of the 41 CIR events were tentatively associated with possible forward or reverse shocks listed in the University of New Hampshire *ACE* Lists of Disturbances and Transients.[6]

The CIR events used in this survey were chosen over the period 1997 November 1 through 2007 June 1. To be included, events had to display a dispersionless intensity increase of at least 24 hr duration that coincided with an increase in solar wind speed typical of entering a fast solar wind stream. Solar wind temperature, density, and magnetic field strength were also examined in the selection of periods. In order to obtain reasonable statistical accuracy for the particle measurements, we also required that the peak 230–320 keV nucleon^{-1} He intensity exceed 10 particles s^{-1} cm^2 sr MeV nucleon^{-1}. A number of candidate events were discarded, since there was possible contamination from SEPs. For times through the end of 2004, all the CIRs in the survey (except No. 22) were included in the comprehensive list from Jian et al. (2006), who selected events on the basis of plasma and field data. Figure 1 shows a sample event with *ACE* SWEPAM solar wind speed, ULEIS O intensities, and a particle arrival spectrogram that illustrates the dispersionless nature of the event. Although there is a clear jump in solar wind speed, there is no clearly formed shock; however, a possible reverse shock at ~08:30 UT is noted in the *ACE* disturbances list cited above. In the middle panel of Figure 1, note that the traces for different energy O nuclei remain approximately equally spaced, except at the lowest energies, where they become more closely spaced late in the event, a sign of modest spectral hardening (e.g., Reames et al. 1997).

[6] Available at http://www.ssg.sr.unh.edu/mag/ace/ACElists/obs_list.html#shocks.

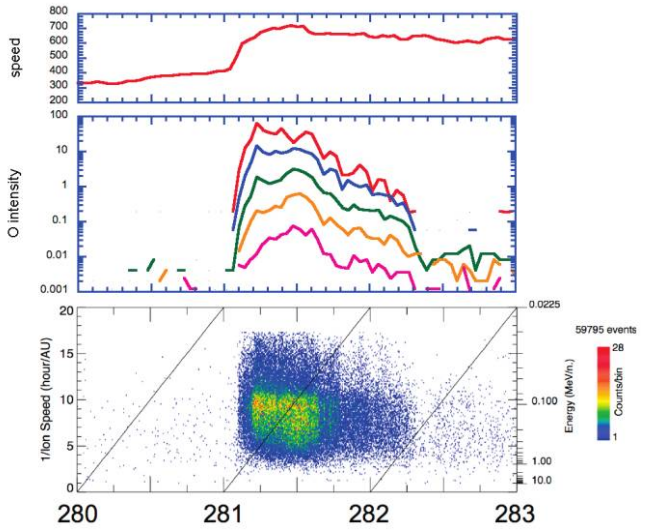

FIG. 1.—Example of CIR event identification for the event of 2005 October 8 (event 26). *Top*: Solar wind speed showing entry into a high-speed stream early on day 281. *Middle*: O intensities from 48 to 770 keV nucleon^{-1} with traces separated by factors of 2 in energy nucleon^{-1}. *Bottom*: Spectrogram of >8 amu ions showing dispersionless onset.

Table 1 lists the 41 CIR events selected. Columns (2)–(5) list the start time and duration of periods when the O intensities were well above background levels. Column (6) lists the peak hourly averaged solar wind speed during the CIR period. Abundances listed in columns (7) and (9)–(11) were summed over the entire event, terminating the sum when the intensities receded to pre-event background levels or another particle event began. Column (7) lists the ^{3}He/^{4}He ratio over the energy range 0.5–2.0 MeV nucleon^{-1}, where the instrument resolution for He isotopes is optimal. Columns (8)–(11) list the peak ^{4}He intensity and ratios of major species compared to O for 0.32–0.45 MeV nucleon^{-1} ions. Columns (12)–(14) contain fitted power-law spectral indices for He differential energy spectra discussed in more detail below.

Figure 2 (*left*) shows the ULEIS mass peaks for C–Fe summed over the energy band (0.32–0.45 MeV nucleon^{-1}) used for measuring abundances; all the ion peaks are clearly resolved, and the statistical accuracy is high. Abundance values for each CIR were obtained by summing over each peak and are listed for major species in Table 1. The right panel of the figure shows the mass histogram for He, with the blue histogram showing all events (*right-hand scale*) and the red line (*left-hand scale*) with a greatly expanded scale showing the ^{3}He peak. The He data are at a somewhat higher energy than the element data in order to optimize the resolution. The ULEIS He isotope resolution in CIRs is better than for large SEP events due to lower count rates in the instrument. The ^{3}He/^{4}He ratio for each CIR was obtained by forming a histogram of the kind shown in Figure 2 (*right*) and then doing a simple linear background interpolation under the ^{3}He peak region. The errors for the ^{3}He/^{4}He ratio values in Table 1 include the statistical uncertainty introduced by this background subtraction, and finite values are reported only if the ratio is at least 2 standard deviations above background and visual inspection of the histogram is consistent with a finite ^{3}He abundance. Sixteen events in Table 1 (~40%) have finite values of ^{3}He; we note that the visual inspection of He histograms suggested that there were additional events with ^{3}He present, so this percentage is probably conservative.

Figure 3 shows properties of the CIRs in relation to the solar cycle. The top panel shows the ^{3}He/^{4}He ratios and compares them with the solar wind average value. In most cases the ^{3}He/^{4}He ratio

TABLE 1

COROTATING INTERACTION REGION EVENTS

EVENT (1)	START YEAR (2)	START DAY (3)	START DAY OF YEAR (4)	LENGTH (days) (5)	PEAK VEL. SOL. WIND (km s^{-1}) (6)	^{3}He/^{4}He 0.5–2.0 MeV nucleon^{-1} × 1000 (7)	0.32–0.45 (MeV nucleon^{-1})				He SPECTRAL INDEX[a]			NOTES (15)
							Peak ^{4}He Intensity (8)	^{4}He/O (9)	C/O × 100 (10)	Fe/O × 100 (11)	0.16–0.91 (MeV nucleon^{-1}) (12)	0.91–3.6 (MeV nucleon^{-1}) (13)	3.4–9.7 (MeV nucleon^{-1}) (14)	
1.....	1998	Jul 16	197.25	2.00	607	...	12.3	...	112 ± 12	2.1 ± 1.2	3.57 ± 0.02	...	...	
2.....	1998	Jul 23	204.00	1.50	732	1.8 ± 0.7	11.1	...	81 ± 11	5.5 ± 2.3	2.90 ± 0.03	2.58 ± 0.29	6.15 ± 0.18	
3.....	1999	Mar 1	60.75	1.75	535	1.9 ± 0.9	16.3	309 ± 18	88 ± 8	4.9 ± 1.3	3.12 ± 0.01	4.98 ± 0.41	...	
4.....	1999	May 18	138.25	1.50	660	...	29.9	258 ± 15	82 ± 7	5.9 ± 1.3	3.95 ± 0.02	...	...	
5.....	1999	Aug 16	228.25	1.50	645	2.4 ± 0.8	20.9	244 ± 11	84 ± 6	6.7 ± 1.2	3.27 ± 0.01	4.63 ± 0.37	...	
6.....	1999	Oct 11	284.50	1.75	625	...	16.1	150 ± 6	70 ± 5	10.4 ± 1.5	2.14 ± 0.01	4.43 ± 0.23	...	2
7.....	1999	Nov 7	311.25	1.25	613	...	26.1	244 ± 13	91 ± 7	5.6 ± 1.2	3.04 ± 0.01	...	...	1
8.....	1999	Dec 4	338.00	1.25	732	...	50.3	191 ± 5	71 ± 3	18.2 ± 1.1	1.74 ± 0.01	3.41 ± 0.07	6.70 ± 0.08	1
9.....	1999	Dec 30	364.75	3.00	701	0.7 ± 0.2	79.5	230 ± 4	67 ± 2	13.8 ± 0.7	1.69 ± 0.01	2.98 ± 0.04	5.52 ± 0.04	1, 2
10.....	2000	Jan 27	27.50	1.25	763	...	160.2	177 ± 5	63 ± 3	13.5 ± 0.7	2.21 ± 0.01	3.02 ± 0.09	4.94 ± 0.05	1, 2
11.....	2000	Feb 6	37.25	2.00	647	...	18.8	194 ± 9	95 ± 6	6.5 ± 1.1	3.43 ± 0.01	5.71 ± 0.80	...	
12.....	2000	Feb 24	55.00	2.25	776	0.9 ± 0.2	94.3	255 ± 6	77 ± 3	11.8 ± 0.8	1.96 ± 0.01	3.36 ± 0.06	6.15 ± 0.05	1, 2
13.....	2000	Mar 22	82.50	2.00	735	0.8 ± 0.2	78.7	137 ± 2	57 ± 2	12.4 ± 0.5	1.86 ± 0.01	3.13 ± 0.06	4.24 ± 0.04	2
14.....	2000	Dec 7	342.25	3.25	654	0.6 ± 0.2	96.3	368 ± 7	71 ± 2	20.0 ± 0.9	1.89 ± 0.01	4.01 ± 0.07	4.67 ± 0.05	
15.....	2002	Mar 30	89.75	3.25	788	...	37.4	190 ± 4	74 ± 2	16.9 ± 0.9	1.65 ± 0.01	3.79 ± 0.06	7.26 ± 0.07	
16.....	2002	Nov 21	325.50	1.50	724	0.9 ± 0.4	58.5	237 ± 7	77 ± 4	12.9 ± 1.0	2.65 ± 0.01	5.05 ± 0.23	...	3
17.....	2003	Feb 15	46.50	2.00	699	2.2 ± 0.6	13.4	287 ± 11	82 ± 5	9.9 ± 1.3	2.22 ± 0.01	4.00 ± 0.15	6.47 ± 0.12	
18.....	2003	Jul 26	207.75	1.25	769	...	1166.2	204 ± 6	86 ± 3	12.2 ± 0.8	2.85 ± 0.02	6.56 ± 0.38	9.38 ± 0.20	
19.....	2003	Aug 21	233.50	2.00	778	1.8 ± 0.6	11.7	290 ± 12	84 ± 5	10.9 ± 1.6	2.25 ± 0.01	4.31 ± 0.20	6.25 ± 0.15	
20.....	2003	Sep 17	260.00	2.50	810	1.0 ± 0.2	78.0	287 ± 6	82 ± 3	10.0 ± 0.6	2.14 ± 0.01	3.26 ± 0.07	6.49 ± 0.05	
21.....	2003	Nov 10	314.25	1.50	775	...	7.0	273 ± 16	79 ± 7	7.6 ± 1.8	2.99 ± 0.02	...[b]	...[b]	
22.....	2003	Nov 14	318.50	3.00	806	...	475.6	195 ± 3	77 ± 2	3.3 ± 0.2	2.38 ± 0.01	...	...[b]	
23.....	2004	Feb 12	43.25	1.50	706	...	41.2	292 ± 10	78 ± 4	10.1 ± 1.1	2.43 ± 0.01	4.04 ± 0.16	7.89 ± 0.22	3
24.....	2004	Nov 20	325.60	1.40	619	...	28.7	318 ± 22	85 ± 9	7.7 ± 1.9	4.03 ± 0.02	5.05 ± 0.89	...[b]	
25.....	2005	Mar 6	65.50	2.00	778	1.2 ± 0.4	17.9	349 ± 14	66 ± 4	15.9 ± 1.8	1.37 ± 0.01	3.12 ± 0.07	5.73 ± 0.06	
26.....	2005	Oct 8	281.00	1.50	716	1.9 ± 0.6	168.5	281 ± 8	87 ± 4	6.8 ± 0.6	2.76 ± 0.02	4.74 ± 0.30	5.78 ± 0.19	
27.....	2005	Nov 30	334.00	3.00	744	...	16.6	307 ± 12	75 ± 4	11.0 ± 1.4	1.50 ± 0.01	3.88 ± 0.10	3.84 ± 0.09	
28.....	2005	Dec 27	361.50	1.25	704	...	20.8	334 ± 14	82 ± 5	13.2 ± 1.8	2.72 ± 0.01	4.81 ± 0.31	...	
29.....	2006	Apr 9	99.25	1.50	681	...	17.3	250 ± 11	61 ± 4	8.7 ± 1.4	1.68 ± 0.01	4.33 ± 0.18	...	
30.....	2006	Jul 31	212.50	2.00	622	...	6.4	279 ± 22	81 ± 9	3.4 ± 1.6	3.01 ± 0.02	...	...	
31.....	2006	Aug 7	219.25	2.25	626	...	6.6	276 ± 18	75 ± 7	4.6 ± 1.5	2.77 ± 0.02	5.36 ± 0.56	...	
32.....	2006	Aug 27	239.75	1.75	656	...	6.1	241 ± 19	60 ± 8	6.9 ± 2.2	3.26 ± 0.02	5.41 ± 1.13	...[b]	
33.....	2006	Sep 24	267.00	1.25	656	...	51.0	294 ± 11	69 ± 4	4.4 ± 0.7	3.08 ± 0.01	6.06 ± 0.50	...	
34.....	2006	Oct 20	293.50	2.50	637	...	27.2	275 ± 10	67 ± 4	6.3 ± 0.9	2.71 ± 0.01	5.40 ± 0.34	...	
35.....	2007	Jan 1	1.75	2.75	688	...	7.9	349 ± 19	72 ± 6	7.7 ± 1.7	2.26 ± 0.01	4.89 ± 0.30	...	4
36.....	2007	Jan 29	29.50	1.40	693	1.8 ± 0.5	52.8	339 ± 10	65 ± 3	5.5 ± 0.7	2.59 ± 0.01	4.35 ± 0.18	4.11 ± 0.09	4
37.....	2007	Feb 13	44.50	3.50	740	1.6 ± 0.5	12.5	351 ± 15	66 ± 4	6.0 ± 1.2	2.05 ± 0.01	5.19 ± 0.23	...	4
38.....	2007	Feb 27	58.75	1.75	679	...	20.2	279 ± 11	61 ± 4	5.7 ± 1.1	2.44 ± 0.01	5.54 ± 0.38	...	4
39.....	2007	Mar 12	71.75	3.25	703	0.8 ± 0.4	33.5	363 ± 12	75 ± 4	7.3 ± 1.0	1.73 ± 0.01	4.16 ± 0.11	...	4
40.....	2007	May 7	127.75	2.00	640	...	59.3	367 ± 12	75 ± 4	5.3 ± 0.8	2.50 ± 0.01	5.96 ± 0.32	...	
41.....	2007	May 18	138.25	1.25	635	...	6.7	376 ± 30	64 ± 8	5.0 ± 1.9	2.08 ± 0.02	5.09 ± 0.39	...	

NOTES.—(1) Event in study of Morris et al. (2001) and Möbius et al. (2002). (2) Event in study of Kucharek et al. (2003). (3) Event in study of Richardson et al. (2006). (4) Event in study of Leske et al. (2008).

[a] Spectral fit to $dJ/dE \propto E^{-\gamma}$ (see discussion in text).

[b] High-energy data influenced by SEP activity.

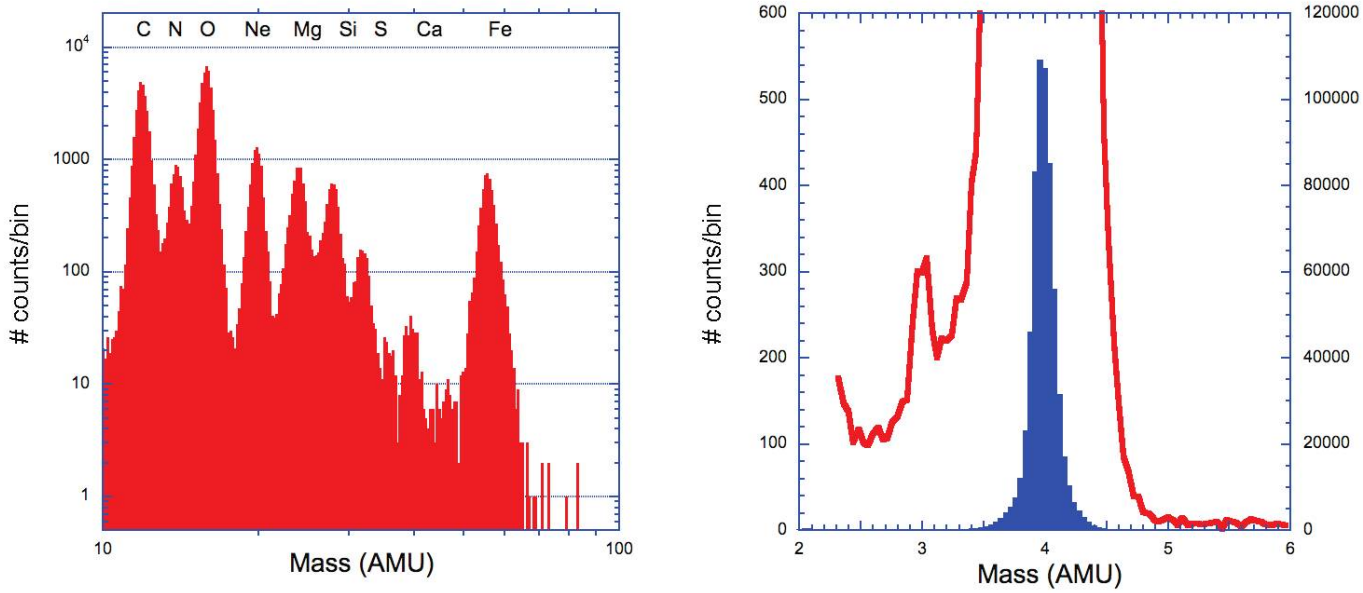

FIG. 2.—ULEIS mass histograms summed over all CIR events in the survey. *Left*: 0.32–0.45 MeV nucleon^{-1} C–Fe; *Right*: 0.5–2.0 MeV nucleon^{-1} ^{4}He peak (*blue histogram, right scale*) and expanded region showing ^{3}He peak (*red line, left scale*).

is enhanced more than twice the solar wind value, with the maximum enhancement being ~6 times the solar wind value. The middle panel shows the 0.32–0.45 MeV nucleon^{-1} peak He intensity; although the two events with the highest intensity occurred during solar active periods, there is little correlation of this intensity with solar activity level as measured by sunspot number. The bottom panel shows the time of each event during each 27 day Bartels solar rotation. Recurrent event series can be seen in late 1999–early 2000, near the end of 2003, and in 2006–2007.

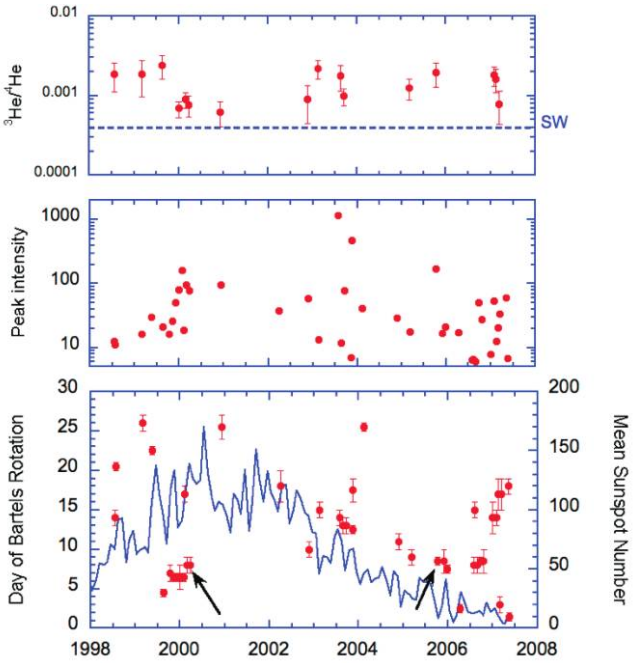

FIG. 3.—*Top*: 0.5–2.0 MeV nucleon^{-1} ^{3}He/^{4}He ratio for events in the survey; ~40% of the events have measurable ^{3}He. The dashed blue line shows the average solar wind value (Gloeckler & Geiss 1998). *Middle*: Peak 0.32–0.45 MeV nucleon^{-1} He intensity for each CIR event. *Bottom*: CIR event times within each 27 day Bartels solar rotation (*red circles*) and the monthly mean sunspot number from the NOAA Web site (*blue line*). The arrows mark events 13 and 26, discussed in text and shown in Fig. 6.

There is a tendency for the higher peak intensities to be associated with the recurrent series. Similar properties were also seen in the survey of higher energy data by Richardson et al. (1993).

2.3. *Average Abundances*

Table 2 lists the 0.385 MeV nucleon^{-1} unweighted average abundances for all species for the 41 CIRs in the survey, and Figure 4 plots these values along with slow and fast solar wind stream average abundances. In addition to the statistical uncertainties given elsewhere, the uncertainty in Table 2 for He includes a 26% systematic uncertainty that is due to the variations in He detection efficiency during the time period of the survey (see Desai et al. 2003 for more details). Heavier element uncertainties include a 2% systematic efficiency uncertainty. Except for Ca, which has not been reported in earlier surveys of CIR abundances, the CIR abundances for C and heavier nuclei in Table 2 agree within the stated uncertainties with earlier surveys at comparable energy (Mason et al. 1997) and with numerous surveys at higher energies (e.g., McGuire et al. 1978; Christon & Simpson 1979; Gloeckler et al. 1979; Scholer et al. 1979; Reames et al. 1991; Richardson et al. 1993). Among the CIR surveys cited, there is a range of He abundance that may be related to the phase of the solar cycle (Richardson et al. 1993). It can be seen from Figure 4 that with the exception of He and Ne the CIR average abundances compare very closely to solar wind abundances, with a slightly closer agreement between the CIRs and the fast solar wind. Compared to the fast solar wind, He and Ne are overabundant in the CIRs by factors of 3.8 ± 1.5 and 2.9 ± 0.4, respectively; other elements show smaller deviations that exhibit no systematic trend with mass.

2.4. *Spectral Forms and Temporal Variations*

Figure 5 shows sample energy spectra for major heavy-ion species in two CIRs. In both cases, the spectra roll over above a few MeV nucleon^{-1}, as reported previously (Mason et al. 1997). The left panel of the figure shows spectra from the 2000 March 22 event (No. 13), where the heavy-ion spectra extend up to ~30 MeV nucleon^{-1} before merging with galactic and anomalous cosmic-ray spectra. The right panel shows the event of 2005 October 8

TABLE 2

MEAN HEAVY-ION ABUNDANCES FOR CIR EVENTS AND OTHER POPULATIONS

Element	CIRs[a] (0.385 MeV nucleon^{-1})	CIRs[b] (5–12 MeV nucleon^{-1})	Slow Solar Wind[c] (~1 keV nucleon^{-1})	Fast Solar Wind[d] (~2 keV nucleon^{-1})	IP Shocks[e] (~0.75 MeV nucleon^{-1})	Large SEPs[f] (0.385 MeV nucleon^{-1})	Impulsive SEPs[g] (0.385 MeV nucleon^{-1})	Photosphere[h]	Corona[i] (~1.4×10^6 K)
^{4}He	273 ± 72	159 ± 10	95.9 ± 28.8	72.7 ± 21.8	44.4 ± 14.4	75.0 ± 23.6	54 ± 14	162 ± 14	126 ± 11
C.....	0.760 ± 0.023	0.890 ± 0.036	0.670 ± 0.067	0.710 ± 0.080	0.368 ± 0.004	0.361 ± 0.012	0.322 ± 0.003	0.501 ± 0.058	0.490 ± 0.056
N.....	0.143 ± 0.005	0.140 ± 0.014	0.069 ± 0.021	0.143 ± 0.016	0.142 ± 0.002	0.119 ± 0.003	0.129 ± 0.002	0.138 ± 0.022	0.123 ± 0.020
O.....	1.000 ± 0.020	1.000 ± 0.037	≡1	≡1	≡1	≡1.0 ± 0.02	≡1.0 ± 0.006	≡1.0 ± 0.161	≡1.0 ± 0.161
Ne.....	0.206 ± 0.009	0.170 ± 0.016	0.091 ± 0.027	0.071 ± 0.010	0.172 ± 0.003	0.152 ± 0.005	0.261 ± 0.003	0.151 ± 0.021	0.191 ± 0.026
Mg.....	0.148 ± 0.006	0.140 ± 0.014	0.147 ± 0.030	0.108 ± 0.022	0.243 ± 0.004	0.229 ± 0.007	0.370 ± 0.003	0.072 ± 0.009	0.224 ± 0.026
Si.....	0.095 ± 0.005	0.100 ± 0.012	0.167 ± 0.034	0.088 ± 0.014	0.213 ± 0.003	0.235 ± 0.011	0.409 ± 0.004	0.071 ± 0.007	0.214 ± 0.022
S	0.028 ± 0.002	0.050 ± 0.008	0.049 ± 0.010	0.035 ± 0.004	0.050 ± 0.001	0.059 ± 0.004	0.118 ± 0.015	0.032 ± 0.008	0.032 ± 0.008
Ca.....	0.007 ± 0.001	...	0.017 ± 0.003	0.007 ± 0.003	0.022 ± 0.002	0.022 ± 0.002	0.060 ± 0.003	0.005 ± 0.0001	0.013 ± 0.0002
Fe.....	0.088 ± 0.007	0.097 ± 0.011	0.120 ± 0.024	0.067 ± 0.007	0.236 ± 0.010	0.404 ± 0.047	0.950 ± 0.005	0.061 ± 0.006	0.186 ± 0.017

[a] This work, based on 41 CIR events observed with *ACE* ULEIS; ^{4}He abundance is averaged over event numbers 3–41.
[b] From Reames (1995); He abundance from 1–4 MeV nucleon^{-1}, heavier ions from 5–12 MeV nucleon^{-1}.
[c] From von Steiger et al. (2000), except Ca from Wurz et al. (2003).
[d] ^{4}He from von Steiger et al. (2000); C–Fe from Gloeckler & Geiss (2007).
[e] From Desai et al. (2003).
[f] From Desai et al. (2006c).
[g] From Mason et al. (2004).
[h] From Lodders (2003).
[i] From Feldman & Widing (2003).

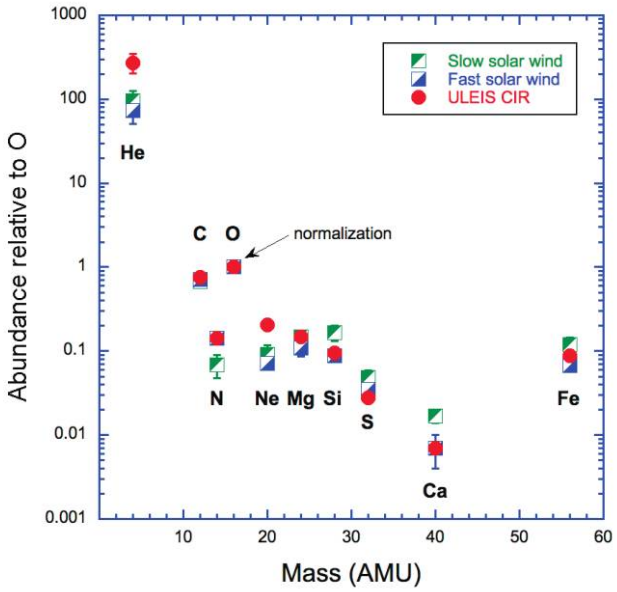

FIG. 4.—Average 0.32–0.45 MeV nucleon^{-1} CIR abundances (*circles*) normalized to O and compared to average solar wind values (von Steiger et al. 2000; Wurz et al. 2003; Gloeckler & Geiss 2007) from slow speed streams (*green half-filled squares*) and fast streams (*blue half-filled squares*).

(No. 26), which is even more intense than the 2000 March 22 event at lower energies; however, the spectra from event 26 are steeper at all energies, and above a few MeV nucleon^{-1} we detected only CIR He. The presence of higher energy particles in event 13 may be related to the fact that this CIR was seen repeatedly on successive solar rotations (see Fig. 3), and so had been present for a much longer time than event 26, which had been seen only on one or two previous rotations. Alternatively, it might be that since the coronal hole responsible for event 13 was much larger than that for event 26, the parent shock structure had a larger size that was responsible for the higher intensities.

The spectral forms shown in Figure 5 are typical of those observed in the survey and are qualitatively similar to the form predicted by the analytical models of Fisk & Lee (1980; see also Jones & Ellison 1991). Written in terms of differential intensity per nucleon used for the data discussed here, the Fisk & Lee spectral form *at the CIR shock* is

$$j(v) = N_0 v^{-n} \exp\left(\frac{-v}{v_0}\right), \quad (1)$$

where j is the differential intensity, v is the particle speed, N_0 is the normalizing constant, and n and v_0 are the low-energy slope and rollover speed, respectively. Equation (1) gives generally excellent fits to the spectra (see also Desai et al. 1999). However, the parameters n and v_0 are not independent of each other, with the result that the fitted values of n and v_0 can be difficult to interpret; for small values of v_0, the "slope" n will be flatter than might be expected, since the exponential term can strongly influence the low-energy slope. Indeed, for some fits, the best-fitted value of n is negative, seemingly implying a positive slope, while in fact the value of v_0 is so small that the decrease in the exponential term ends up producing a negative overall slope in the equation (1) fit.

For this reason, instead of listing fitted values for n and v_0, we fitted power laws $dJ/dE \propto E^{-\gamma}$ over limited energy ranges of the He spectrum, where J is the differential intensity and E is the energy nucleon^{-1}. The lower two energy ranges were from ULEIS data, and the highest one was from SIS (see Table 1). In some cases spectral indices are missing due to inadequate statistics, interference from SEP activity (see table notes), or lack of an increase over Galactic cosmic-ray intensities in the highest energy range. Power laws give very good fits over the energy ranges used.

Figure 6 plots the He spectral indices from Table 1 versus the O spectral index over the same energy range as the lowest energy He points. Several features of the spectra are apparent from the figure. First, the He and O spectra are extremely well correlated when measured over the 0.16–0.91 MeV nucleon^{-1} range. The

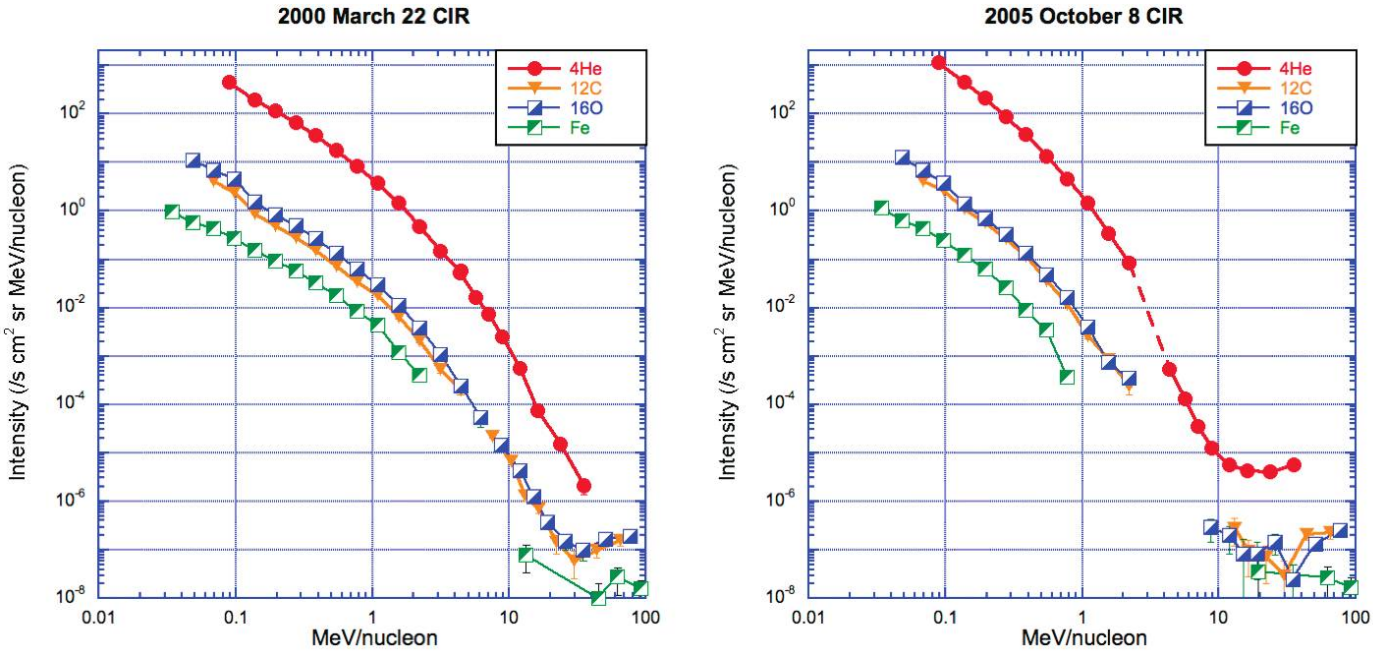

FIG. 5.—ULEIS and SIS spectra for major elements in two sample events (other species are similar). *Left*: Event 13 spectra rolled over at a few MeV nucleon^{-1}, continuing as power laws out to 30 MeV nucleon^{-1}. *Right*: Event 26, more intense at low energies, but rolling over to a very steep spectrum above ~2 MeV nucleon^{-1}. Flat portions of the spectra above ~10 MeV nucleon^{-1} are due to anomalous cosmic rays and Galactic cosmic rays.

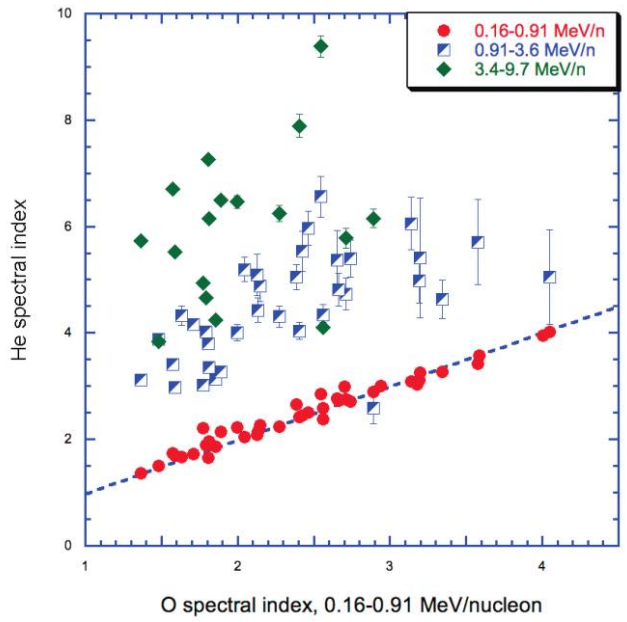

FIG. 6.—He spectral index, γ, for a spectral form $dJ/dE \propto E^{-\gamma}$ over three energy ranges plotted vs. the spectral index for O in the range 0.16–0.91 MeV nucleon^{-1}. The dashed blue line shows a 1 : 1 ratio between the He and O spectral indices.

average of the ratios of spectral indices for the 41 events over this range is $\langle \gamma_{He}/\gamma_O \rangle = 1.03 \pm 0.01$. The half-filled squares in the figure show the He spectral indices for the middle energy range, 0.91–3.6 MeV nucleon^{-1}, where it can be seen that the spectra have steepened by roughly 2 units, with considerable scatter. The only case in which the middle energy range index is about equal to the lowest energy range is from event 2, which was a single power law over the entire ULEIS energy range, and steepened only at SIS energies. Finally, the highest energy spectral points show that the steepening continues above a few MeV nucleon^{-1}, with even more scatter. It is interesting that only events with relatively hard low-energy spectra produce measurable increases in the SIS energy range, showing that the low-energy slope and high-energy cutoff are due to related effects, not two separate processes. We searched for correlation between the spectral indices and peak ^{4}He intensity and found no convincing pattern.

The mean γ values for the He spectra are 2.51 ± 0.10 (41 points), 4.47 ± 0.17 (35 points), and 5.97 ± 0.33 (19 points) for the energy ranges 0.16–0.91, 0.91–3.6, and 3.4–9.7 MeV nucleon^{-1}, respectively. Summing up over all CIR events in a 1982–1986 survey, Richardson et al. (1993) reported $\gamma = 4.11 \pm 0.30$ for 1.9–2.0 MeV nucleon^{-1} He, consistent with the observations reported here for the middle He energy range.

It is clear from Figure 6 that the O and He low-energy spectral forms are very similar, and Figure 7 explores this further for all of the elements observed by plotting the ratio of each species to O. Although there is some variation with energy, the ratios are constant to within a factor of ~2, even though the spectra roll over in the energy range covered, and the intensities (for He and O) change by a factor of $\sim 10^8$. This contrasts strikingly with the observed spectral behavior of SEPs and shock-associated particles, where rollover energies vary significantly from species to species (e.g., Mewaldt et al. 2005a) and the relative abundance ratios show variations of more than 2 orders of magnitude over energy ranges comparable to those studied here (e.g., Mazur et al. 1993; Desai et al. 2003, 2006c; Cohen et al. 2005).

In a number of the events where the He spectral index extended to high energy (see Table 1), the He spectrum showed a clear power-law shape out to >10 MeV nucleon^{-1}. Figure 8 shows two sample events with fits using equation (1), where it can be seen that at the highest energies the data are well above the exponential rollover, so this deviation from the model spectral form is significant. Since the deviation occurs where the measurements transition from ULEIS to SIS, it could be asked whether this is an instrumental effect. However, we do not believe this is the case, since the two instruments agree well over this transition both in CIRs (see also Fig. 5) and in SEP events (e.g., Mewaldt et al. 2005b). Clear deviations such as those shown in the figure were seen only in those cases with relatively hard high-energy spectra, since in cases with steep spectra the energy range covered was too small for a clear test.

Figure 9 shows hourly average Fe/O ratios (*blue squares*) along with He intensities (*red circles*). Panel *a* shows an essentially

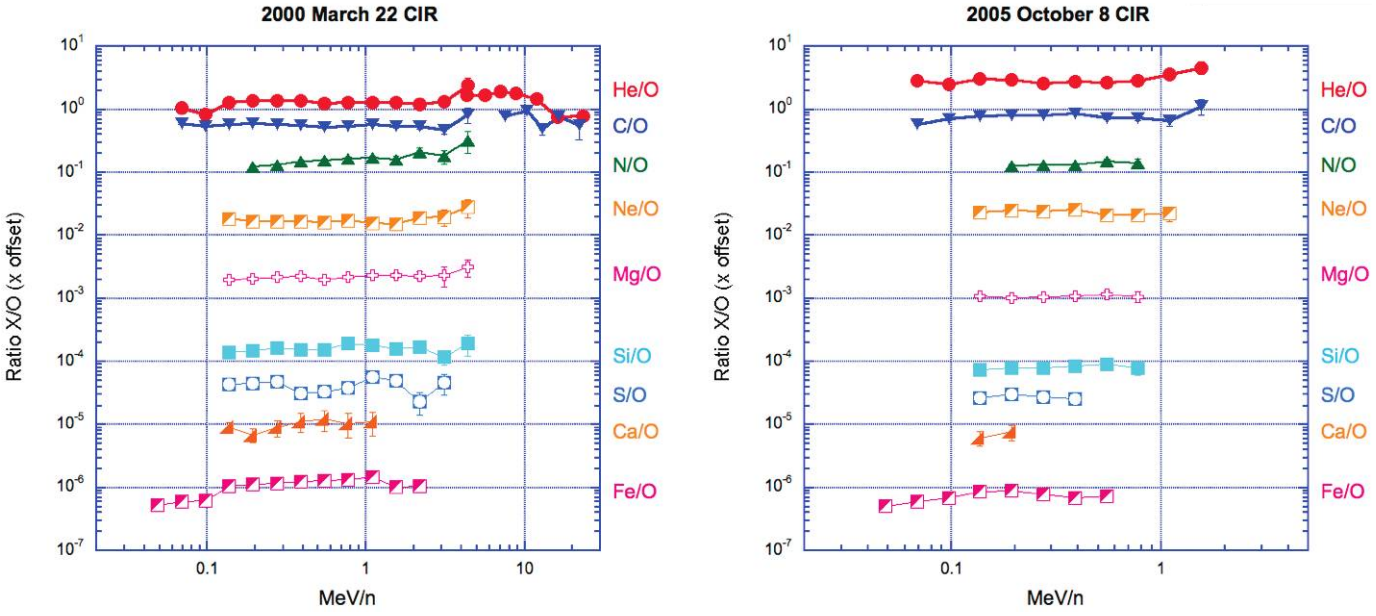

FIG. 7.—Element abundances normalized to O for the two events in Fig. 5. Over the energy range shown the relative abundances are constant to within a factor of ~2, even though the spectra roll over in this range and intensities vary by large factors ($\sim 10^8$ for He and O). Ratios have been offset by constant factors to spread out the data points.

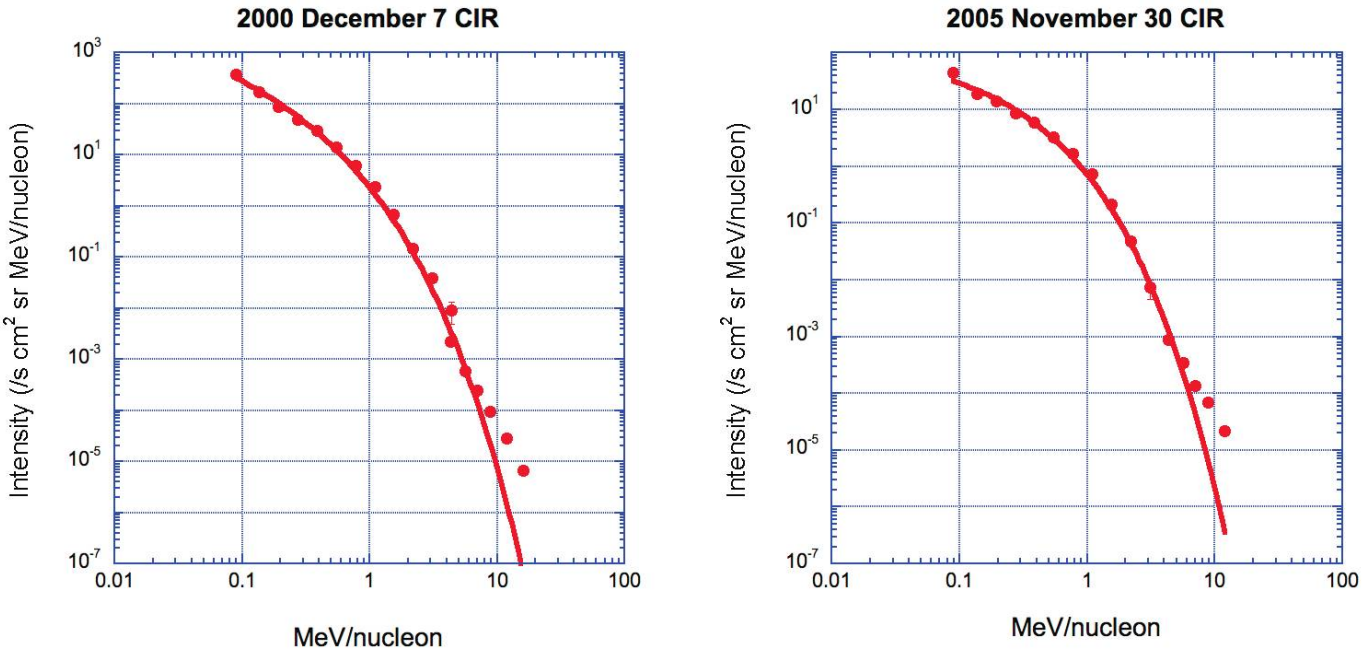

FIG. 8.—Examples of fits of Fisk & Lee (1980) spectral form fits to (*left*) event 14 and (*right*) event 27, showing large deviation from exponential rollover at high energies.

constant Fe/O ratio once the CIR intensity increase is under way; this is the behavior for all events in the survey except for the case shown in (*b*), which shows a definite trend rise in Fe/O as the event progresses. The constancy of Fe/O during the events presumably reflects the nearly steady-state nature of CIRs, at least in comparison with SEP events that routinely show very strong Fe/O temporal variations (e.g., Mason et al. 1983; Tylka et al. 1999; Cane et al. 2003).

2.5. *Event-to-Event Abundance Variations*

Event-averaged abundances for CIRs show event-to-event variations (see Fig. 10). In the figure, the event-averaged ratio of each element with respect to O is plotted versus the Fe/C ratio for that event. In order to separate the data points in the figure, the ratios He/O, Ne/O, Mg/O, Si/O, S/O, Ca/O, and Fe/O have been multiplied by 10^{-X}, where $X = 2, 1, 2, 3, 3, 3$, and 5, respectively. The overall range of Fe/C is a factor of $\sim$15, and if the lowest ratio measurement is removed, the range is a factor of <10, much smaller than the variations seen in large SEP events (Desai et al. 2006c). Systematic features are apparent in the ordering of the variations, e.g., events with high Fe/C also have high Ca/O and S/O ratios. An unexpected feature of the variations is that the He/O and Ne/O ratios show statistically significant negative correlations with Fe/C—something not observed for elements of

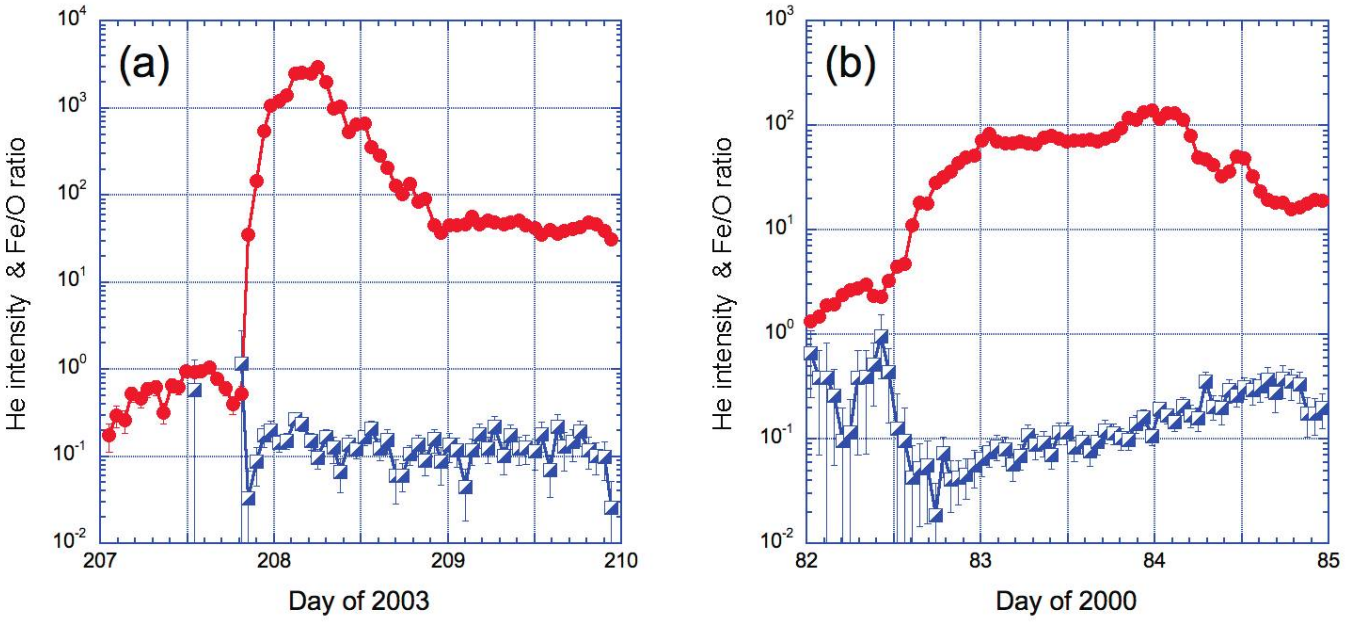

FIG. 9.—Time variations of hourly average 0.32–0.45 MeV nucleon^{-1} He intensity (*red circles*) and Fe/O ratio (*blue squares*) for (*a*) event 18 and (*b*) event 13. Variations in Fe/O during the CIR in (*b*) were highly unusual; most events show no time variation in the Fe/O ratio, as in (*a*).

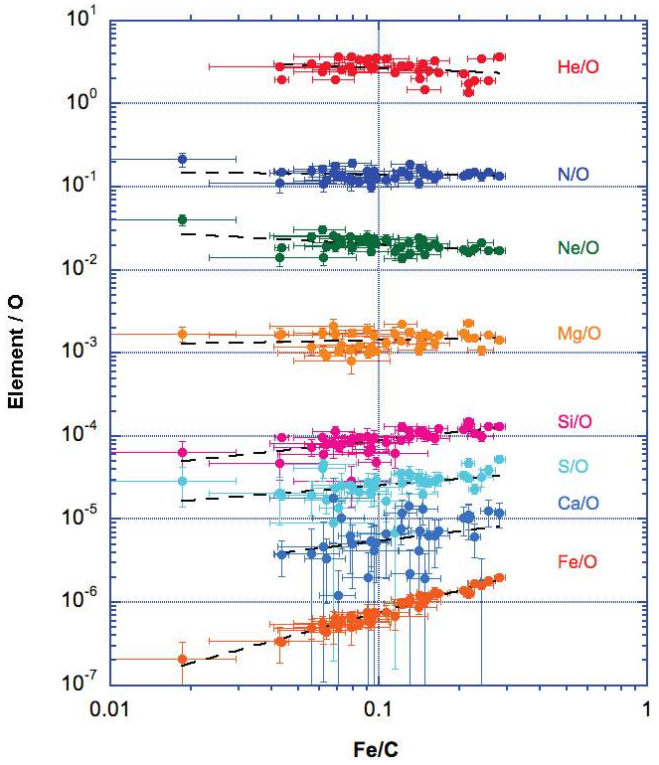

FIG. 10.—Average value of 0.32–0.45 MeV nucleon^{-1} abundance of elements normalized to O vs. Fe/C ratio. Elements have been multiplied by an offset factor (see text) to avoid crowding. The dashed lines are power-law fits for each element.

nearby mass, such as N/O or Mg/O. This anticorrelation is not caused by systematics of solar wind composition between fast and slow streams, since Fe, He, and Ne are all more abundant in the slow solar wind than in fast streams (von Steiger et al. 2000). Examining the events individually, it turns out that the Fe/C ratio for the first few events in the survey is lower than in later events, and that the He/O and Ne/O ratios are higher than observed later on, so the negative correlation might be a temporal effect. Possibly this could be due to a solar cycle effect (e.g., see Desai et al. 2006b), but given the relatively small number of CIRs this is uncertain.

Two previous surveys of CIR abundances have reported variations in relative abundance that correlate with the solar wind speed during the event (Richardson et al. 1993; Mason et al. 1997). Table 3 summarizes these previous results, showing where positive, negative, or no correlation was reported. Entries in the table marked "?" were described by the authors as possibly significant. We examined this further for He, C, Ne, Mg, Si, and Fe abundances relative to O as a function of peak solar wind speed for all the events in this survey. Since the present survey has many more events (41 vs. <15) and much better statistical accuracy than previous surveys, it allows a more stringent test for trends. For He/O, C/O, Ne/O, and Mg/O the current data revealed no significant trends; i.e., the correlation coefficients had probabilities of ~10%–30% of being from a random distribution. The Si/O ratio showed a significant positive correlation (0.41) in our data (the probability of being from a random population <1%), in contrast to the earlier cited surveys, which both found no correlation of Si/O versus solar wind speed. Fe/O also showed a significant positive correlation (0.47) with solar wind speed that was not seen or was unclear in the earlier studies. In summary, we detect significant positive correlations of Si/O and Fe/O with solar wind speed, but this result is not corroborated by earlier studies, so we consider the overall evidence for abundances depending on solar wind speed to be unproven.

TABLE 3
CORRELATION OF CIR ABUNDANCES WITH SOLAR WIND SPEED

Mean Energy (MeV nucleon^{-1})	He/O	C/O	Ne/O	Mg/O	Si/O	Fe/O
2.35[a]	+	+	...	−?	...	−
0.150[b]	...	+	+	...	...	+?
0.385[c]	...	...	...	...	+	+

[a] Richardson et al. (1993).
[b] Mason et al. (1997).
[c] This work.

The event-to-event variations in CIR ratios, such as Fe/O shown in Figure 10, range over a factor of ~10, very much larger than the long-term averaged solar wind Fe/O ratio, which varies by less than a factor of 2 between slow and fast solar wind streams (see Table 2). However, over shorter periods of time, solar wind abundance variations are much larger (von Steiger et al. 1995; Raymond et al. 2001) and are comparable in size to the event-to-event CIR variations shown in the figure. Figure 11 explores the correlation between solar wind Fe/O with CIR Fe/O on an event-by-event basis. The Fe/O ratio was chosen for this comparison because it shows larger variation than other ratios and is relatively easy to obtain for the solar wind data. Since CIR acceleration is presumed to peak beyond Earth orbit, the seed population for the energetic particles at 1 AU is presumably from solar wind or suprathermals beyond Earth orbit. If convected out with the solar wind, the seed particles would have passed Earth orbit before the CIR was observed at 1 AU. So, in comparing with solar wind abundances, Figure 11 shows the correlation coefficient between the Fe/O ratio in each of the 41 CIRs, compared with the solar wind Fe/O ratios measured over time periods of the same length as each CIR averaging interval, but offset to an earlier time. The solar wind Fe/O was calculated using 2 hr average values of Fe/O from the level 2 data at the *ACE* Science Center Web site,[7] summed over each CIR period and offset by the amount shown. The top left panel of the figure shows that the correlation between the Fe/O ratio in the CIRs versus the preceding solar wind is low if the offset is small (essentially measuring the solar wind at the same time as the CIR), but it grows smoothly with increasing offset length, reaching a peak when comparing the CIR Fe/O with the solar wind Fe/O between 2 and 4 days prior to the CIR. The bottom left panel shows the probability that the calculated correlation coefficient would be exceeded by a random population; for 2–4 day offsets this probability is very small. Figure 11 (*right*) shows the case for a 4 day offset, where each point is the average from a single CIR. Although there is significant scatter, the panel shows that the high correlation coefficient is not caused by one or two particular cases.

2.6. *Summary of Observations*

The main properties observed in our survey of the 0.32–0.45 MeV nucleon^{-1} heavy ions for 41 CIR events can be summarized as follows:

1. Spectral forms of heavy ions can be fitted with broken power laws where below ~1 MeV nucleon^{-1} the average slope is 2.51 ± 0.10, steepening to an average slope of 4.47 ± 0.17 in the range ~1–3 MeV nucleon^{-1}. At higher energies, the spectra further

[7] See http://www.srl.caltech.edu/ACE/.

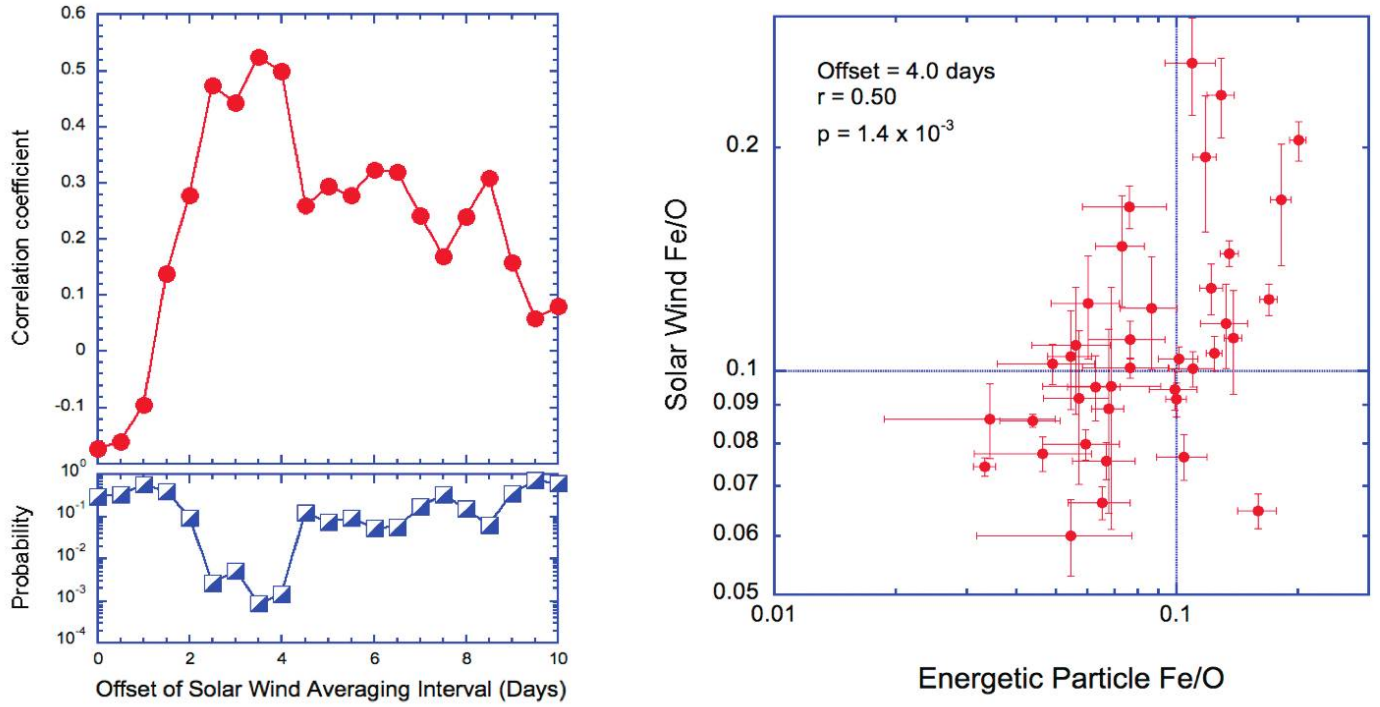

FIG. 11.—*Top left*: Correlation coefficient between average Fe/O for energetic particles in each CIR vs. Fe/O in the solar wind measured from 0 to 10 days earlier than the CIR period. *Bottom left*: Probability that the correlation coefficient would be exceeded by a sample from a random population. *Right*: Energetic particle vs. solar wind Fe/O for the case of a 4 day offset.

steepen but remain a power law in many cases, inconsistent with the exponential rollover generally predicted in models.

2. The average abundances of all species show little variation over the energy range <0.1 to a few MeV nucleon^{-1}, so the spectral shapes are very similar.

3. Most CIR events show no systematic temporal abundance variations during the course of the event.

4. The ^{3}He/^{4}He ratio over the range 0.5–2.0 MeV nucleon^{-1} is enhanced compared to solar wind values in $\sim$40% of the events, up to a factor of $\sim$6 times the solar wind abundance.

5. The average abundances compared to O of elements over the range He–Fe are close to the averages for the fast solar wind, with the exception of He and Ne, which are overabundant by factors of 3.8 ± 1.5 and 2.9 ± 0.4, respectively.

6. Previously reported positive correlations of CIR He/O, C/O, and Ne/O with solar wind speed are not found in this survey; we find that Si/O and Fe/O correlate positively with solar wind speed, but this was not observed in the previous studies and so is open to question.

7. The event-to-event variations of average abundance show a variation of a factor of $\sim$10 for ratios such as Fe/C and considerably less for species closer together in mass.

8. The average Fe/O ratio in each CIR is well correlated with the Fe/O ratio in the solar wind 2–4 days preceding the CIR.

3. DISCUSSION

3.1. *Acceleration Mechanisms and Seed Population*

Many aspects of the heavy-ion species observed in our survey are consistent with predictions of models of steady-state diffusive acceleration at CIR shocks beyond Earth orbit, such as that of Fisk & Lee (1980) and others cited above. The similarity of spectral forms over a very wide intensity range and the almost universal lack of temporal abundance variations during an event fit well into the model predictions. The calculated spectral forms of a low-energy power law rolling over at higher energies are also generally good representations of the data. The correlation between the 320–450 keV nucleon^{-1} Fe/O ratio and the solar wind Fe/O ratio 2–4 days preceding the CIR reported here implies that the 320–450 keV nucleon^{-1} energetic particle source is roughly 2–4 days of slow solar wind travel time beyond 1 AU. At typical 300–400 km s^{-1} slow solar wind speeds, this corresponds to a heliocentric distance of $\sim$1.3–2 AU, which is less than the $\sim$3–4 AU distances at which CIR intensities are at a maximum (e.g., Van Hollebeke et al. 1978). We note that this simple treatment of the observations in the ecliptic plane does not reflect the three-dimensional structure of CIRs or possible deviations from simple field-aligned transport from the acceleration region (Dwyer et al. 1997), and so they should be considered illustrative only.

At the lowest energies (below $\sim$100 keV nucleon^{-1}), however, it is difficult for ions accelerated in the outer heliosphere to propagate upstream in the solar wind to reach Earth. Equation (1) is the Fisk & Lee (1980) prediction *at the location* of the CIR shock; their predicted spectra at 1 AU include an additional factor involving distance to the shock (their eq. [6]), and this additional term becomes very small for particle speeds below $\sim$100 keV nucleon^{-1} (see discussion in Mason et al. 1999b). The predicted rollover in the spectrum is not apparent in the data presented here, and observations at even lower energies than those reported here show that CIR spectra continue smoothly as power laws down to solar wind energies (Chotoo et al. 2000). This problem was explored by Giacalone & Jokipii (2002), who showed that compression regions associated with CIRs near 1 AU could energize particles without the presence of shocks, so the low-energy particles may originate locally. Figure 12 compares one of their previously published calculations with the He spectrum in event 13. The agreement is quite reasonable considering that the parameters

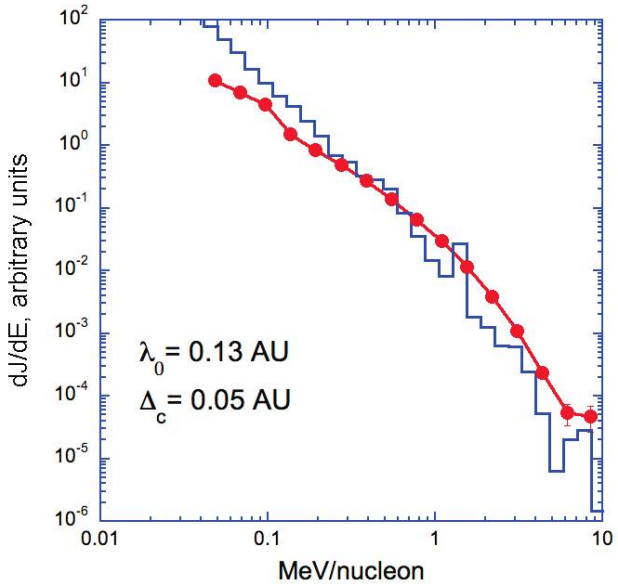

FIG. 12.—Event 13 He spectrum (*red circles*) compared with the CIR spectrum (*blue histogram*) calculated with the acceleration model using solar wind compression regions for a mean free path λ_0 of 0.13 AU and transition region width Δ_C of 0.05 AU (for details see Giacalone et al. 2002).

chosen by Giacalone & Jokipii were nominal and not optimized for the event shown. While the observational data from deep space probes make it clear that the highest CIR intensities occur beyond 1 AU where the shocks are well-formed, it appears probable that particles with energies below ~100 keV nucleon^{-1} are accelerated close to 1 AU.

Recently, Fisk & Gloeckler (2006) described a mechanism of accelerating particles by stochastic acceleration in compressional turbulence in the solar wind. This mechanism, which could be expected to be relevant to CIRs, produces a low-energy power law with a spectral index of 1.5, which at some higher energy rolls over to a steeper spectrum. The prediction of a specific spectral index is a feature of this model that differs from the earlier models where the spectral index depends on the compression ratios in the CIR shocks and which generally did not give accurate predictions on a case-by-case basis (Desai et al. 1999). Figure 6 shows that there is no clustering of the spectral indices near 1.5, although it might be significant that only one or two cases lie somewhat below it. Since the Fisk & Gloeckler (2006) spectral index is for a steady-state acceleration, the presence of steeper spectra at low energies might be an indication that equilibrium has not been reached.

Several CIRs in this study that accelerated He to >10 MeV nucleon^{-1} showed a clear power-law form at high energies that is inconsistent with the exponential forms predicted by analytical (Fisk & Lee 1980; Jones & Ellison 1991) and numerical models cited above (Giacalone et al. 2002). Power-law spectral forms extending to energies where the spectra merged with the cosmic-ray spectrum at tens of MeV nucleon^{-1} have also been reported for H and He (Richardson et al. 1993 and references therein; Mason et al. 1997). Thus, while the spectral forms reported here generally show the rollover predicted near ~1 MeV nucleon^{-1} by the models, the high-energy spectral form is different. This may be related to the seed population assumption used in the models. For example, Fisk & Lee (1980) assumed a seed population that was a delta function in energy; Giacalone et al. (2002) assumed pickup ions were the seed population, and these typically show a sharp cutoff at twice the solar wind speed. If in fact the seed population is a power law in energy, such as given in the model by Fisk & Gloeckler (2006) and generally observed in IP space (Gloeckler 2003), the spectral form at high energies could be affected, producing a harder spectrum.

3.2. *Abundances and Seed Population*

The models of CIR acceleration cited above assume a suprathermal seed population in order for the initial particle speeds to be sufficiently large to allow the particles to interact multiple times with the accelerating shock or compression region. There is also strong observational evidence for a suprathermal seed source, due to the presence of ions in CIRs that are extremely rare in the bulk solar wind. The first such ion detected in CIRs was singly ionized He, which at 1 AU consists of 10%–20% of the total He (Hilchenbach et al. 1999; Chotoo et al. 2000; Möbius et al. 2002), and at several AU He^+ dominates the CIR He abundance (Gloeckler et al. 1994). During individual CIR events at 1 AU the He^+ abundance increases with time during the event, presumably due to improving the magnetic connection between 1 AU and increasingly efficient portions of the distant shock (Morris et al. 2001). The presence of He^+ in such relatively large quantities and showing an increase with radial distance from the Sun is strong evidence for a pickup ion source at speeds above the bulk solar wind.

The ^{3}He reported here at levels well above the solar wind ^{3}He/^{4}He ratio in some CIRs is also an indicator that the bulk solar wind is not the direct source of the energized material. Remnant suprathermal ^{3}He from impulsive SEP events is often present in the IP medium (Mason et al. 1999a; Wiedenbeck et al. 2005), where it can be further accelerated in shock-associated SEP events and by traveling IP shocks (Desai et al. 2001, 2003, 2004, 2006c). About 40% of the events in the current survey have measurable ^{3}He, which is similar to the occurrence frequency observed in large SEP events, although the SEP events sometimes show enhancements much larger than those seen in CIRs (up to a factor of ~150 enhancement vs. a maximum enhancement of a factor of ~6 in this survey). However, since the ^{4}He abundance in our survey is ~3.5 times larger than that in the SEP survey of Desai et al. (2006a), a lower ^{3}He/^{4}He ratio may not be surprising. In addition, the fact that CIR particles are energized further from the Sun than SEPs may play a role.

The relatively large abundances of trace constituents He^+ and ^{3}He show the importance of suprathermals in the CIR seed population. This raises the question regarding the reason that the major CIR constituents, especially C, O, and Fe, have relative abundances very close to the solar wind, and indeed the CIR Fe/O ratio is well correlated with Fe/O temporal variations in the solar wind preceding the event. A self-consistent scenario for these observations is simply that the CIR C, O, and Fe seed population is primarily heated bulk solar wind, so these suprathermals reflect the bulk population of the solar wind. Gloeckler (2003) has presented direct observations of ubiquitous suprathermal tails on the solar wind distribution, even for periods when there are no shocks that would cause temporary heating and acceleration. The mechanism of Fisk & Gloeckler (2006) describes a process that could cause the heating and acceleration. The Fisk & Gloeckler (2006) and previously cited CIR acceleration models using diffusive acceleration can produce particle spectra that are independent of species type, and so the fact that the CIR Fe/O is close to that in the solar wind is important. This contrasts strongly with Fe/O in IP shock events where Fe is depleted compared to the

seed population (Desai et al. 2003). In summary, it appears that CIR energetic particles are accelerated out of a suprathermal particle population consisting primarily of heated solar wind, with additional amounts of pickup ions and remnant impulsive SEP material.

The He and Ne abundances, however, remain a puzzle. In the case of He, previous surveys have noted its high abundance compared to solar wind and SEPs (e.g., Scholer et al. 1979; Reames et al. 1991; Richardson et al. 1993; Fränz et al. 1999). In the current survey, we also report an overabundance of Ne along with the odd additional behavior that the Ne/O ratio is anticorrelated with variations in the Fe/C ratio from event to event (Fig. 10). Since both He and Ne are elements with high ionization potentials that allow their interstellar neutrals to penetrate deeper into the heliosphere than other species in this study, and since pickup He is clearly accelerated in CIRs, it might seem that the He and Ne abundances are due to the presence of pickup ions, which are identifiable because they are singly charged. Although CIR He and Ne both show more single charge state material than other heavy ions (Mazur et al. 2002; Möbius et al. 2002), the absolute amount of He^+ and Ne^+ is only 25% and 8%, respectively, much too small to explain the factors of $\sim$2–4 overabundance reported here. We note that a possible role of the so-called inner source material within $\sim$0.25 AU of the Sun is also inconsistent with these ionization state measurements, since the inner source material would be singly ionized (Gloeckler et al. 2000; Schwadron et al. 2000).

3.3. C/O *in CIRs versus* C/O *in Solar Energetic Particles and Interplanetary Shocks*

It has long been known that the CIR C/O ratio is considerably higher than the C/O ratio in SEP events (Scholer et al. 1979; Reames et al. 1991). These early studies noted that the CIR C/O tended to resemble the Galactic cosmic-ray ratio of $\sim$1, and the SEPs resembled the solar atmosphere. Given this view, the CIR C/O ratio was puzzling. We now have accurate measurements of the solar wind C/O ratio, which turns out to be very close to the CIR C/O ratio. This fact, taken together with the Fe/O and suprathermal ion properties discussed above, provides a natural explanation for the observed value of C/O in CIRs. Many have pointed out that the relatively low C/O ratio in SEPs is close to photosphere C/O, as well as C/O in the solar upper atmosphere (Feldman & Widing 2003), which is a more plausible site for SEP material.

This raises a question regarding traveling IP shocks, which also have a low C/O ratio ($<$0.4) and whose heavy-ion abundances resemble SEPs generally (Desai et al. 2003). How could traveling IP shocks produce a significantly different C/O ratio than CIR shocks? Given the similarity in mass and mass-to-charge ratio for SEP- and CIR-accelerated C and O, it is difficult to envision an acceleration mechanism that would produce a factor of $\sim$2 fractionation in these elements without simultaneously producing huge fractionation in other elements whose mass-to-charge ratio is much different, and this is not seen. This points to the seed population as the origin of this difference. In the case of SEPs, the energetic particles are clearly accelerated out of a suprathermal seed population that originates very close to the Sun where the C/O is smaller (Desai et al. 2006a). Likewise, for traveling IP shock events, the seed population must also originate much closer to the Sun than generally assumed, since it would need to come from regions or sources where the suprathermal coronal-like abundances, not the solar wind, are dominant. The results of Desai et al. (2004) are consistent with this assertion, as they show that the IP shocks probably reaccelerated suprathermal-through-energetic seed spectra that were previously accelerated in impulsive and gradual SEP events rather than directly out of the solar wind (see also Mewaldt et al. 2006).

In order to account for the differences in the CIR and SEP abundances, we can clearly point to differences in the seed population, i.e., suprathermal solar wind material for CIRs and coronal material for SEP events, with varying amounts of other suprathermal material such as remnant impulsive SEPs and interstellar pickup ions. However, an interesting question that does arise but essentially remains unanswered from the new composition measurements obtained over the last decade with *ACE* and *Ulysses* is, why is the solar wind composition so different from coronal abundances?

4. SUMMARY AND CONCLUSIONS

We have surveyed the heavy-ion composition, spectra, and temporal variations in 41 CIR events with *ACE* spectrometers with mass resolution and statistical precision much greater than previous studies. The energy spectral shapes and temporal variation fit reasonably well with existing analytical models in which the particles are energized by diffusive shock acceleration beyond Earth orbit. However, at energies below $\sim$100 keV nucleon^{-1}, the presence of power-law spectra suggests a more local source due to compressional acceleration, since such particles cannot easily propagate inward from several AU. Although the observed spectra roll over at a few MeV nucleon^{-1} as predicted by the models, we find that for the cases in which the high-energy spectra can be measured over a broad energy range, they are power laws, not the exponentials predicted by models. It may be that this is evidence that the seed population itself is a power law and does not have the sharp velocity cutoff usually assumed in the models.

The rare isotope ^{3}He is present in about 40% of the CIRs, with significant enhancements over the solar wind ^{3}He abundance. The presence of this rare isotope, in addition to previously reported He^+, shows that CIR energetic particles contain ions that are extremely rare in the solar wind, indicating that the CIR seed population is primarily composed of suprathermal ions. Comparing the Fe/O ratio in each CIR with the solar wind Fe/O ratio, we find that there is a strong correlation if the comparison is done with solar wind that passed by *ACE* 2–4 days before the CIR. We conclude that the main heavy elements C, O, and Fe in CIRs are derived from suprathermals that originated in heated solar wind. This requires a heating mechanism that operates throughout the solar cycle, even in quiet periods, such as the turbulent cascade mechanism proposed by Fisk & Gloeckler (2006). Compared to the solar wind, He and Ne are overabundant in CIRs by a factor of $\sim$3, which suggests a pickup ion source. However, pickup He and Ne should be singly ionized if this is the case, and this is not observed, so these abundances remain anomalous. Finally, a long-standing puzzle about a "high" C/O ratio in CIRs is now resolved, since it turns out that the CIR C/O ratio is very close to the solar wind value and presumably close to the heated solar wind suprathermal source. The low C/O in interplanetary shocks suggests that traveling interplanetary shocks and SEPs accelerate seed particles that originate very close to the Sun, where coronal abundances dominate the suprathermal population.

We thank the many individuals at the University of Maryland and the Johns Hopkins Applied Physics Laboratory who

constructed the ULEIS instrument. We thank the *ACE* SWEPAM and MAG teams for solar wind speed and magnetic field data used here, as well as their list of transients and disturbances maintained on the *ACE* Science Center Web site. J. Giacalone kindly provided the numerical fit data used in Figure 12. Sunspot numbers were obtained from the NOAA Web site at the National Geophysical Sciences Data Center, ftp://ftp.ngdc.noaa.gov/STP/SOLAR_DATA/SUNSPOT_NUMBERS. This work was supported in part by NASA under grant NNG04GJ51G at the Johns Hopkins University Applied Physics Laboratory.

REFERENCES

Cane, H. V., von Rosenvinge, T. T., Cohen, C. M. S., & Mewaldt, R. A. 2003, Geophys. Res. Lett., 30, 8017
Chotoo, K., et al. 2000, J. Geophys. Res., 105, 23107
Christon, S. P., & Simpson, J. A. 1979, ApJ, 227, L49
Cohen, C. M. S., Stone, E. C., Mewaldt, R. A., Desai, M. I., von Rosenvinge, T. T., & Wiedenbeck, M. E. 2005, J. Geophys. Res., 110, A09S16
Desai, M. I., Marsden, R. G., Sanderson, T. R., Balogh, A., Forsyth, R. J., & Gosling, J. T. 1998, J. Geophys. Res., 103, 2003
Desai, M. I., Mason, G. M., Dwyer, J. R., Mazur, J. E., Smith, C. W., & Skoug, R. M. 2001, ApJ, 553, L89
Desai, M. I., Mason, G. M., Mazur, J. E., & Dwyer, J. R. 2006a, Space Sci. Rev., 124, 261
———. 2006b, ApJ, 645, L81
Desai, M. I., et al. 1999, J. Geophys. Res., 104, 6705
———. 2003, ApJ, 588, 1149
———. 2004, ApJ, 611, 1156
———. 2006c, ApJ, 649, 470
Dwyer, J. R., Mason, G. M., Mazur, J. E., Jokipii, J. R., von Rosenvinge, T. T., & Lepping, R. P. 1997, ApJ, 490, L115
Feldman, U., & Widing, K. G. 2003, Space Sci. Rev., 107, 665
Fisk, L. A., & Gloeckler, G. 2006, ApJ, 640, L79
Fisk, L. A., & Jokipii, J. R. 1999, Space Sci. Rev., 89, 115
Fisk, L. A., & Lee, M. A. 1980, ApJ, 237, 620
Forsyth, R. J., & Marsch, E. 1999, Space Sci. Rev., 89, 7
Fränz, M., Keppler, E., Lauth, U., Reuss, M. K., Mason, G. M., & Mazur, J. E. 1999, Geophys. Res. Lett., 26, 17
Giacalone, J., Jokipii, J. R., & Kóta, J. 2002, ApJ, 573, 845
Gloeckler, G. 1999, Space Sci. Rev., 89, 91
———. 2003, in AIP Conf. Proc. 679, Solar Wind Ten, ed. M. Velli, R. Bruno, & F. Malara (New York: AIP), 583
Gloeckler, G., Fisk, L. A., Geiss, J., Schwadron, N. A., & Zurbuchen, T. H. 2000, J. Geophys. Res., 105, 7459
Gloeckler, G., & Geiss, J. 1998, Space Sci. Rev., 84, 275
———. 2007, Space Sci. Rev., 130, 139
Gloeckler, G., Hovestadt, D., & Fisk, L. A. 1979, ApJ, 230, L191
Gloeckler, G., et al. 1994, J. Geophys. Res., 99, 17637
———. 1998, Space Sci. Rev., 86, 497
Gosling, J. T., & Pizzo, V. J. 1999, Space Sci. Rev., 89, 21
Hilchenbach, M., Grünwaldt, H., Kallenbach, R., Klecker, B., Kucharek, H., Ipavich, F. M., & Galvin, A. B. 1999, in AIP Conf. Proc. 471, Solar Wind Nine, ed. S. R. Habbal et al. (New York: AIP), 605
Horbury, T. S., & Schmidt, J. M. 1999, Space Sci. Rev., 89, 61
Jian, L., Russell, C. T., Luhmann, J., & Skoug, R. M. 2006, Sol. Phys., 239, 337
Jones, F. C., & Ellison, D. C. 1991, Space Sci. Rev., 58, 259
Kucharek, H., et al. 2003, J. Geophys. Res., 108, LIS 15-1
Lazarus, A., Richardson, J. D., Decker, R. B., & McDonald, F. B. 1999, Space Sci. Rev., 89, 53
Leske, R. A., et al. 2008, in Proc. 30th Int. Cosmic Ray Conf. (Merida), in press
Lodders, K. 2003, ApJ, 591, 1220
Mason, G. M., Gloeckler, G., & Hovestadt, D. 1983, ApJ, 267, 844
Mason, G. M., Mazur, J. E., & Dwyer, J. R. 1999a, ApJ, 525, L133
Mason, G. M., Mazur, J. E., Dwyer, J. R., Jokipii, J. R., Gold, R. E., & Krimigis, S. M. 2004, ApJ, 606, 555
Mason, G. M., Mazur, J. E., Dwyer, J. R., Reames, D. V., & von Rosenvinge, T. T. 1997, ApJ, 486, L149
Mason, G. M., & Sanderson, T. R. 1999, Space Sci. Rev., 89, 77
Mason, G. M., et al. 1998, Space Sci. Rev., 86, 409
———. 1999b, Space Sci. Rev., 89, 327
Mazur, J. E., Mason, G. M., Klecker, B., & McGuire, R. E. 1993, ApJ, 404, 810
Mazur, J. E., Mason, G. M., & Mewaldt, R. A. 2002, ApJ, 566, 555
McComas, D. J., Bame, S. J., Barker, P., Feldman, W. C., Phillips, J. L., Riley, P., & Griffee, J. W. 1998, Space Sci. Rev., 86, 563
McGuire, R. E., von Rosenvinge, T. T., & McDonald, F. B. 1978, ApJ, 224, L87
Mewaldt, R. A., Cohen, C. M. S., & Mason, G. M. 2006, in Solar Eruptions and Energetic Particles, ed. N. Gopalswamy, R. A. Mewaldt, & R. B. Torbert (Geophys. Monogr. 165; Washington: AGU), 115
Mewaldt, R. A., et al. 2005a, in AIP Conf. Proc. 781, The Physics of Collisionless Shocks, ed. G. Li, G. P. Zank, & C. T. Russell (New York: AIP), 227
———. 2005b, J. Geophys. Res., 110, A09S18
Möbius, E., Morris, D., Popecki, M. A., Klecker, B., Kistler, L. M., & Galvin, A. B. 2002, Geophys. Res. Lett., 29, 1
Morris, D., Möbius, E., Lee, M. A., Popecki, M., Klecker, B., Kistler, L. M., & Galvin, A. B. 2001, in AIP Conf. Proc. 598, Solar and Galactic Composition, ed. R. F. Wimmer-Schweingruber (New York: AIP), 201
Raymond, J. C., et al. 2001, in AIP Conf. Proc. 598, Solar and Galactic Composition, ed. R. F. Wimmer-Schweingruber (New York: AIP), 49
Reames, D. V. 1995, Adv. Space Res., 15, 41
Reames, D. V., Ng, C. K., Mason, G. M., Dwyer, J. R., Mazur, J. E., & von Rosenvinge, T. T. 1997, Geophys. Res. Lett., 24, 2917
Reames, D. V., Richardson, I. G., & Barbier, L. M. 1991, ApJ, 382, L43
Richardson, I. G. 2004, Space Sci. Rev., 111, 267
Richardson, I. G., Barbier, L. M., Reames, D. V., & von Rosenvinge, T. T. 1993, J. Geophys. Res., 98, 13
Richardson, I. G., et al. 2006, J. Geophys. Res., 111, A07S09
Scholer, M. 1999, Space Sci. Rev., 89, 105
Scholer, M., Hovestadt, D., Klecker, B., & Gloeckler, G. 1979, ApJ, 227, 323
Schwadron, N. A., Geiss, J., Fisk, L. A., Gloeckler, G., Zurbuchen, T. H., & von Steiger, R. 2000, Geophys. Res. Lett., 105, 7465
Smith, C. W., L'Heureux, J., Ness, N. F., Acuña, M. H., Burlaga, L. F., & Scheifele, J. 1998, Space Sci. Rev., 86, 613
Stone, E. C., Frandsen, A. M., Mewaldt, R. A., Christian, E. R., Margolies, D., Ormes, J. F., & Snow, F. 1998a, Space Sci. Rev., 86, 1
Stone, E. C., et al. 1998b, Space Sci. Rev., 86, 357
Tylka, A. J., Reames, D. V., & Ng, C. K. 1999, Geophys. Res. Lett., 26, 2141
Van Hollebeke, M. A. I., McDonald, F. B., Trainor, J. H., & von Rosenvinge, T. T. 1978, J. Geophys. Res., 83, 4723
von Steiger, R., Wimmer Schweingruber, R. F., Geiss, G., & Gloeckler, G. 1995, Adv. Space Res., 15, 3
von Steiger, R., et al. 2000, J. Geophys. Res., 105, 27217
Wiedenbeck, M. E., et al. 2005, in Proc. 29th Int. Cosmic Ray Conf. (Mumbai), 1, 117
Wurz, P., Bochsler, P., Paquette, J. A., & Ipavich, F. M. 2003, ApJ, 583, 489